APL Materials

Impact of non-ferroelectric phases on switching dynamics in epitaxial ferroelectric $Hf_{0.5}Zr_{0.5}O_2$ films

Cite as: APL Mater. **10**, 031108 (2022); https://doi.org/10.1063/5.0083661
Submitted: 28 December 2021 • Accepted: 17 February 2022 • Published Online: 14 March 2022

Tingfeng Song, Florencio Sánchez and Ignasi Fina

View Online

Export Citation

CrossMark

ARTICLES YOU MAY BE INTERESTED IN

HfO_2-based ferroelectrics: From enhancing performance, material design, to applications
Applied Physics Reviews **9**, 011307 (2022); https://doi.org/10.1063/5.0066607

Ferroelectricity in hafnium oxide thin films
Applied Physics Letters **99**, 102903 (2011); https://doi.org/10.1063/1.3634052

Next generation ferroelectric materials for semiconductor process integration and their applications
Journal of Applied Physics **129**, 100901 (2021); https://doi.org/10.1063/5.0037617

© 2022 Author(s).

APL Materials | ARTICLE | scitation.org/journal/apm

Impact of non-ferroelectric phases on switching dynamics in epitaxial ferroelectric $Hf_{0.5}Zr_{0.5}O_2$ films

Cite as: APL Mater. 10, 031108 (2022); doi: 10.1063/5.0083661
Submitted: 28 December 2021 • Accepted: 17 February 2022 •
Published Online: 14 March 2022

View Online

Export Citation

CrossMark

Tingfeng Song, Florencio Sánchez,[a] and Ignasi Fina[a]

AFFILIATIONS

Institut de Ciència de Materials de Barcelona (ICMAB-CSIC), Campus UAB, Bellaterra 08193, Spain

[a]Authors to whom correspondence should be addressed: ifina@icmab.es and fsanchez@icmab.es

ABSTRACT

Determining the switching speed and mechanisms in ferroelectric HfO_2 is essential for applications. Switching dynamics in orthorhombic epitaxial ferroelectric $Hf_{0.5}Zr_{0.5}O_2$ films with either significant or negligible presence of monoclinic paraelectric phase is characterized. Switching spectroscopy reveals that the polarization dynamics in pure orthorhombic ferroelectric phase films can be modeled by the Kolmogorov–Avrami–Ishibashi mechanism with large characteristic time ($\approx 1\ \mu s$), which is shortened in fatigued junctions. The long switching time indicates that non-archetypical switching mechanisms occur and that ionic motion or other extrinsic contributions might be at play. Films containing a higher amount of paraelectric monoclinic phase show a shorter switching time of 69 ns, even in pristine state, for applied electric field parallel to the imprint field, enabling synaptic-like activity using fast electric stimuli. Thus, the presence of defects or paraelectric phase is found to improve the switching speed, contrary to what one can expect *a priori*.

© *2022 Author(s). All article content, except where otherwise noted, is licensed under a Creative Commons Attribution (CC BY) license (http://creativecommons.org/licenses/by/4.0/).* https://doi.org/10.1063/5.0083661

INTRODUCTION

Renewed interest in ferroelectric materials for memory applications has been triggered by the discovery of ferroelectricity in HfO_2 films,[1] which are compatible with CMOS technology.[2,3] CMOS compatibility makes ferroelectric HfO_2 interesting for memory applications, such as non-volatile random access memories[4] and field effect transistors.[5] Contrary to what is commonly found in archetypical ferroelectric materials where ferroelectric properties degraded while reducing thickness to the nanoscale, ferroelectric hafnium oxide shows stable ferroelectric character in films thinner than around 10 nm.[6–12] This robustness for very thin films makes HfO_2 especially suitable for its integration in ferroelectric tunnel junctions.[13,14]

Polarization switching dynamics characterization is extremely relevant for applications and to understand the underlying mechanisms of ferroelectric switching. In recent years, switching dynamics has been characterized in ferroelectric polycrystalline HfO_2 films having different dopant atoms.[15–17] Commonly, it is found that the characteristic switching time is in the range of 500–1000 ns.[18–26] This characteristic switching time might be largely affected by the characteristic time constant of the measurement setup.[27] However, a record value as fast as 925 ps has been obtained by minimizing the device area and the series resistance contribution.[28–30] Fast switching (around 10 ns) has also been observed in ferroelectric ZrO_2 films.[31,32] It is commonly found that switching dynamics follows Nucleation Limited Switching (NLS) model,[33] as expected for polycrystalline films, contrary to the Kolmogorov–Avrami–Ishibashi (KAI) model[34,35] expected for films of high crystalline quality.[36] It has been reported that the increase of remanent polarization ascribed to the increase of non-pinned ferroelectric orthorhombic domains by doping or electric cycling is correlated with an increase of the characteristic switching time.[22,23] In contrast, the increase of orthorhombic phase, and concomitantly the remanent polarization, by high pressure annealing results in shorter switching time.[37] In contrast and counterintuitively, the increase in the number of defects results in the decrease of the switching time.[26] At the local level, microscopic characterization performed in ferroelectric HfO_2

polycrystalline films indicates that thermodynamic switching can occur,[38,39] in addition to giving hints on the intriguing dependence of the coercive electric field dependence on thickness.[40] Despite the fact that several works (some of them contradictory) have investigated domain dynamics in polycrystalline ferroelectric hafnium oxide, further investigation is needed to fully understand switching dynamics. This is especially important in systems where extrinsic contribution from defects or paraelectric phases is minimized.

Single crystals of ferroelectric HfO_2 would be ideal candidates to characterize intrinsic switching dynamics. However, their growth has only been recently reported, and their functional characterization is still incipient.[41] In contrast, the growth and characterization of epitaxial films has been important in the last few years, and these are very convenient to investigate intrinsic properties of ferroelectric HfO_2.[42] For example, very recently, the direct comparison between the epitaxial $Y:HfO_2$ films on ITO/(111)YSZ and polycrystalline $Y:HfO_2$ films on $Pt/TiO_x/SiO_2/Si$ substrates has allowed to demonstrate that homogeneous nucleation is observed at high electric field in both cases and that the response is slightly slower in the epitaxial ones. At low electric field, defects play a very important role, and thus polycrystalline and epitaxial films' switching dynamics differ, and polycrystalline samples on $Pt/TiO_x/SiO_2/Si$ show a less homogeneous switching than the epitaxial films on ITO/YSZ(111), as expected due to the greater defects amount.[43] The epitaxial growth of ferroelectric doped HfO_2 films is also possible using suitable substrates[44–48] and bottom $La_{2/3}Sr_{1/3}MnO_3$ (LSMO) electrodes,[49] and high polarization, endurance, and retention have been demonstrated in these films. In addition, epitaxial stress determines the relative amount of monoclinic and orthorhombic phases, and it allows the growth of either almost pure orthorhombic ferroelectric films or films having a relative amount of monoclinic phase depending on the selected substrate.[50] Thus, the epitaxial thin films on LSMO electrodes are optimal for the characterization of intrinsic properties and to evaluate in a well-controlled way the impact of defects and particularly of the paraelectric monoclinic phase. Here, instead of comparing the epitaxial and polycrystalline films, we present the direct comparison of switching dynamics in epitaxial 1%La doped $Hf_{0.5}Zr_{0.5}O_2$ (La:HZO) films having pure orthorhombic phase with those of the same composition having a relative amount of monoclinic phase. Pure orthorhombic films are grown on $GdScO_3$ (GSO) substrate and the mixed-phase films on $SrTiO_3$ (STO) substrate. It turns out that the characteristic switching time is around 2 μs in the pure orthorhombic film. Switching spectroscopy analysis reveals that pure orthorhombic phase films follow the KAI switching dynamics, even at very low electric field with domain growth dimensionality between 1 and 2. Instead, the mixed orthorhombic/monoclinic phase films show NLS. It is also observed that the switching time is much shorter for mixed phase films, reaching 69 ns. Therefore, the results indicate that samples having larger fraction of non-ferroelectric phase with concomitant larger number of incoherent domain boundaries show 2 orders of magnitude faster switching time dominated by distributed nucleation and that slow response is intrinsic of the orthorhombic phase.

RESULTS

La:HZO films were grown by pulsed laser deposition on top of 25 nm LSMO buffered (001)-oriented GSO and STO substrates (GSO is indexed here as pseudocubic). We focus on a 7 nm thick film, although measurements of films with different thickness are shown in the supplementary material. 20 nm thick top Pt electrodes of 20 μm diameter were deposited *ex-situ* by DC sputtering at room temperature. Deposition conditions can be found elsewhere.[51]

The XRD 2θ-χ map of a 7 nm thick La:HZO film grown on LSMO/GSO is shown in Fig. 1(a). The most visible spots correspond to GSO substrate and LSMO electrode reflections as labeled. The bright spot located at $\chi = 0^\circ$ and $2\theta = 30.2^\circ$ corresponds to the o-HZO(111) reflection. Other orientations or phases are not detected as thoroughly investigated in similar films.[50,52] Positive-Up-Negative-Down (PUND) measurements [Fig. 1(b)] confirmed the ferroelectric character of the film. The current vs applied voltage loop exhibits two clear switching peaks. The integrated polarization loop shows that remanent polarization is 14.6 $\mu C/cm^2$ and the coercive voltages are 2.6 and −3.1 V, denoting the presence of imprint field toward LSMO bottom electrode.

Thus, the epitaxial film on the GSO substrate shows negligible quantity of spurious phases, and $P_r = 15\ \mu C/cm^2$. Next, we present switching dynamics characterization. The pulse train used is described in supplementary material S1. In Fig. 1(c), the dependence of switched polarization (ΔP) on switching pulse duration (τ_w) is shown for different amplitude positive writing pulses (V_w). It can be observed that the switching starts at around 200 ns ($V_w = 4$ V) and that, for decreasing voltage, the onset switching time does not vary but ΔP is reduced, as expected. ΔP values are obtained after subtracting residual leakage current contribution (as described in supplementary material S2), already observed in archetypical ferroelectric materials,[53] arising from the complex coexisting electronic and ionic[54–56] leakage mechanisms present in HfO_2 films, which result in hysteretic leakage current (as shown in supplementary material S3). It might be also argued that this additional contribution comes from additional ferroelectric switching with different switching dynamics, which is unlikely due to saturation not been identified. In any case, this contribution is not removable from ΔP value obtained by PUND, and from now on, we will focus our analysis on the dynamics of the switchable contribution, in which saturation is observed. We have fitted the data using the KAI model equation $\Delta P = \Delta P_s * (1 - e^{-(\tau_w/\tau_0)^n})$, where τ_0 is the characteristic switching time, n is the dimensionality exponent, and ΔP_s is the saturated switched polarization. For the maximum applied voltage of 4 V, the fitting parameters are $\tau_0 = 1.4\ \mu$s and n = 1.6 (fitting parameters extracted at other voltages are in supplementary material S4). τ_0 is longer to what is commonly obtained in polycrystalline ferroelectric hafnium oxide films. Usually at low electric field, deviations from intrinsic switching can be observed due to the more relevant role of defects.[43] This is not observed here; thus, the switching is intrinsic at any voltage, and the role of defects is negligible. The obtained n > 1 indicates mixture of 1D and 2D domain wall propagation. For decreasing applied voltage, τ_0 and n slightly increase (supplementary material S4), as commonly found in other ferroelectric materials.[57] In any case, the switching data of the epitaxial La:HZO films on the GSO substrate are well described by the KAI model.

In Fig. 1(d), the dependence of ΔP on switching τ_w is shown for different $V_w < 0$ pulses. We obtain $\tau_0 = 2.5\ \mu$s and n = 1.0. It can be observed that τ_0 is larger than for positive voltages. This is expected due to the mentioned negative imprint field. In addition to

© Author(s) 2022

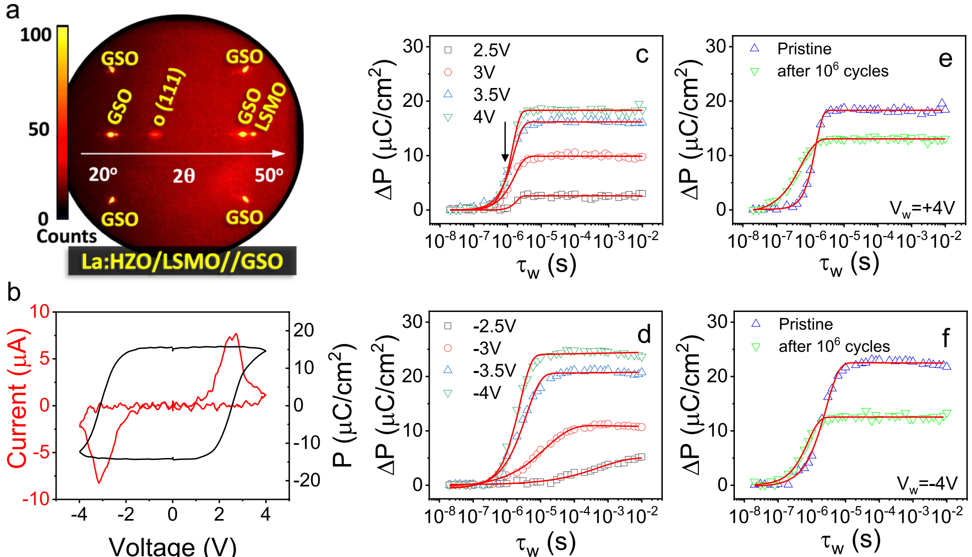

FIG. 1. (a) XRD 2θ-χ map of the La:HZO/LSMO/GSO sample. (b) Current–voltage loop and corresponding polarization–voltage loop of the same sample measured at 10 kHz and maximum voltage of 4 V. Dependence of ΔP on τ_w after (a) positive and (b) negative V_w pulses of the indicated amplitude. ΔP dependence on τ_w after (c) positive and (d) negative V_w pulses in the pristine state and after 10^6 bipolar cycles. Red lines are the fitting of the data by the KAI model.

the τ_0 increase, we observe a decrease in n, which being near 1 indicates that 1D domain wall propagation dominates. This asymmetry in domain wall propagation mode has been observed in other ferroelectric oxides, and it is attributed to asymmetric defect distribution in films along the out-of-plane direction[58] also at the origin of the imprint field.

In Figs. 1(e) and 1(f), the ΔP dependence on τ_w is shown for a different capacitor measured in the same sample in the pristine state and after 10^6 cycles at 4 V. First, it can be observed that the maximum polarization is reduced in the cycled junction. This is due to the fatigue effect (supplementary material S5), which results from the pinning of ferroelectric domains due to defects redistribution, charge injection, or transformation of the orthorhombic to monoclinic phase.[59,60] Interestingly, τ_0 decreases from τ_0 = 1.4 and 2.5 μs to 0.55 and 0.77 μs for positive and negative polarity, respectively. For negative polarity, n does not significantly change being 1.1 after cycling, but it decreases from 1.6 to 1.1 for positive polarity. Therefore, the formation of pinned domains or non-ferroelectric phases by electric cycling results in a faster switching speed and an average reduction of the domain growth dimensionality. This conclusion can also be extracted from the direct measurement of the current switching (supplementary material S6).

To directly infer the role of non-ferroelectric phases in the domain switching dynamics, we characterize a La:HZO/LSMO film of same thickness (7 nm) grown on STO. The 2θ-χ map of this sample is shown in Fig. 2(a). In contrast to the map of the La:HZO/LSMO/GSO sample [Fig. 1(a)], there is an additional reflection corresponding to the non-ferroelectric monoclinic phase. Accordingly, the ferroelectric character of the sample remains, but the remanent polarization is reduced to 12.6 μC/cm^2, as shown by the I–V and the P–V loops in Fig. 2(b). The coercive voltage has also been reduced (being now 2.28 and −3.06 V), and the imprint field increased compared to the La:HZO/LSMO/GSO sample. The ΔP dependence on τ_w for different positive voltages is shown in Figs. 2(c) and 2(d). ΔP values obtained prior leakage subtraction are shown in supplementary material S7. It can be observed that, even

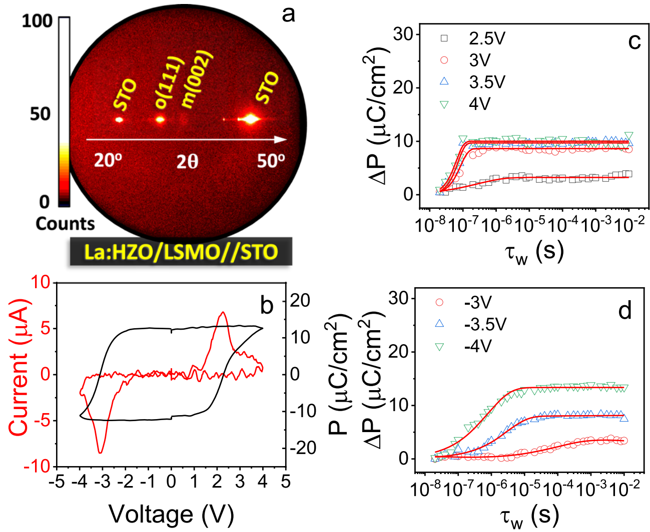

FIG. 2. (a) XRD 2θ-χ map of the La:HZO film on STO substrate. (b) I–V loop and corresponding P–V loop of the same sample measured at 10 kHz and maximum voltage 4 V. Dependence of ΔP on (c) positive and (c) negative switching V_w pulses with different amplitudes. Red lines are the fitting of the data by the KAI model.

© Author(s) 2022

for the shortest applied switching pulse (20 ns), some switchable charge appears and τ_0 = 69 ns is obtained. This extracted switching time is limited by the time constant of the experimental setup, which is around 100 ns (supplementary material S8). Note that, because the experimental setup limits τ_0, the fittings do not correspond to the KAI model and only to an exponential dependence. For negative voltage, τ_0 increases (supplementary material S4) to 820 ns and n = 0.5 for −4 V. The larger τ_0 compared to the value corresponding to positive voltage is expected because the imprint field is against polarization switching, thus limiting the stability of switched domains along this particular direction.[58] We note that other films with thickness ranging from 4.5 to 13 nm show similar switching dependence on τ_w (supplementary material S9). Electric cycling also results in a reduction of τ_0 for the film grown on STO as for the one on GSO, although there is only a minute improvement in the STO case (supplementary material S10). Most notable is that n is <1 for V_w < 0, which indicates that the KAI model is not valid. Therefore, we proceed to the data fitting using the NLS model for data collected at −4 V. As shown in supplementary material S11, the data are properly fitted by the NLS model. For comparison, the fitting using the NLS model were also used for the La:HZO/LSMO/GSO sample (supplementary material S11). Note the fact that the data collected in the films grown on GSO can be fitted with the NLS model, which can be expected due to NLS model being an extended version of the KAI model, when the distribution of switching times (function "F" in supplementary material S11) is not a delta function.[61] Thus, remarkably fast switching (τ_0 = 69 ns) and failure of KAI model to describe the switching dynamics are observed in the epitaxial La:HZO film with the coexistence of orthorhombic and monoclinic phases.

Overall, it has been shown that (i) switching dynamics in agreement with KAI model with n near to 2 is observed for the nominally single orthorhombic phase film, (ii) switching dynamics in agreement with NLS model is observed for the film showing coexisting orthorhombic/monoclinic phases, (iii) faster switching time is observed in films showing larger presence of non-ferroelectric or non-switchable phase induced by a different substrate or by electric field cycling, and (iv) faster switching time is observed if switching is aligned with the imprint field.

In Figs. 3(a) and 3(b), we summarize the main result of this study. Whereas orthorhombic rich film on GSO does not show ferroelectric switching using τ_w = 50 ns [Fig. 3(a)], in the film on STO, the switching is present by an amount of near ΔP = 4 $\mu C/cm^2$ [Fig. 3(b)]. Similar comparison at different τ_w is shown in supplementary material S12. The aperture in the latter PUND loop indicates back switching during the delay time between pulses, which does not preclude the observation of polarization contrast. The observed switching at 50 ns is a benchmark for ferroelectric hafnium oxide films, only overpassed by data obtained in ultrafast characterization setups (see summary Table S1 in supplementary material S13). Highly relevant is that with increasing film quality, switching becomes slower. The slow switching in films on GSO is correlated with the less abundant defects, whereas in films on STO, charged defects help on the initiation of the nucleation. In fact, films grown on STO show larger leakage than the film grown on GSO, indicating the larger presence of defects (supplementary material S14). The small abundance of defects produces that different nucleation points in the sample are equally probable, and thus, KAI switching dynamics with single characteristic time occurs. This result is in agreement with that

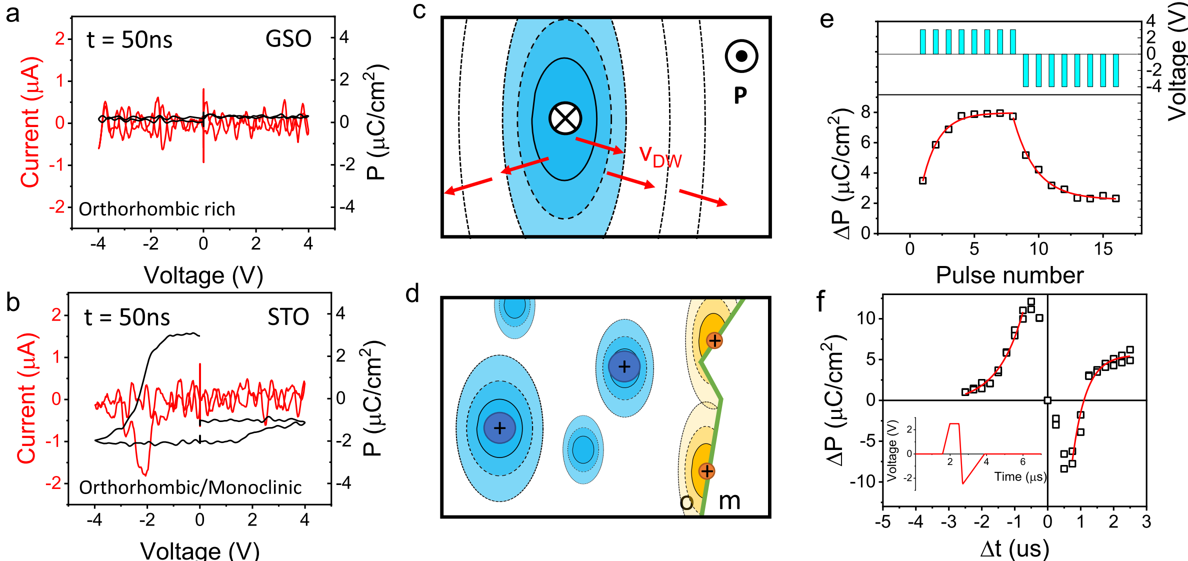

FIG. 3. I–V and P–V loops showing the polarization switching of single orthorhombic phase (a) and mixed orthorhombic/monoclinic phase (b) films after applying a voltage pulse of τ_w = 50 ns. Top-view sketch for the nucleation and growth process in (c) single orthorhombic phase and (d) mixed orthorhombic/monoclinic phase films. Black outward and inwards arrows account for polarization and red arrows for the domain wall propagation in panel c. (e) Dependence of polarization state in the La:HZO film on STO on the applied number of pulses of 50 ns width of opposite polarity (+3/−4 V). (f) Dependence of polarization state in La:HZO film on STO on the Δt of two consecutive pulse of synaptic-like shape (inset) of 750 ns FWHM and Δt step of 250 ns.

© Author(s) 2022

reported slower response of epitaxial (with expected lower amount of defects) compared with polycrystalline films.[43]

In addition, the absence of defects favors 2D domain growth as sketched in Fig. 3(c) (top view), in agreement with the higher n coefficient. However, defects are not inexistent, and they produce non-negligible imprint electric field, asymmetric domain growth propagation, and n < 2 even for high electric fields; features are not present in the epitaxial thin films of archetypical ferroelectrics, such as PZT[36] or $BiFeO_3$.[62] In addition, τ_0 in these ferroelectric oxides is, in general, below microseconds.[36] Thus, τ_0 (≈ 1 μs) in single orthorhombic phase films grown on GSO is in comparison long. This long characteristic time is compatible with the participation of ionic motion processes for the domain switching nucleation and expansion,[63,64] as found in other oxides.[65] The oxygen vacancies, most likely to be present, have mobility of $\approx 10^{-12}$ cm^2 V^{-1} s^{-1},[66–68] which at 4 V and for a sample thickness of 7 nm gives a τ_0 in the order of a second. This time is much larger than τ_0 disregarding ionic motion across the film. Instead, one can expect that oxygen motion can be relevant at the interfaces, where the effects might be faster. Note also that τ_0 in pure orthorhombic films is also longer than that found in the epitaxial films grown by post-annealing crystallization.[43] This is related to the higher remanent polarization of the films reported here, indicating greater presence of orthorhombic phase and thus slower switching.

Films on STO are more abundant in defects, and charged defects do help in the initiation of the nucleation, allowing its occurrence at shorter τ_0. These defects, mainly at the electrode interfaces [positive blue charges in Fig. 3(d)] or at the monoclinic/orthorhombic interfaces [positive orange charges in Fig. 3(d)], locally generate different built-in electric fields, resulting in a distribution of switching times, and thus, NLS switching well describes the growth kinetics. τ_0 is as a consequence shorter. In this latter case, ionic motion can also play a relevant role, but the fast switching kinetics indicates that it must be local and not dominating the domain dynamics.

Recently, it has been shown that ferroelectric HfO_2 films can show memristive characteristics,[13,44,52,70–72] which allows mimicking the brain synapse[14,43,46] using voltage pulses of very diverse shape in the range of 1–100 μs. Thus, the fast switching can be useful to develop fast neuromorphic like devices. In Fig. 3(e) and 3(f), demonstration of potentiation/depression and Spike-Timing-Dependent Plasticity (STDP) neuromorphic-like behavior in the La:HZO/STO film is shown. In Fig. 3(e), the ΔP is measured during application of defined number of positive (+3 V) and negative (−4 V) pulses of 50 ns time width (see top panel). The pulse amplitude asymmetry is required to obtain symmetric potentiation/depression curves. It can be observed a gradual increase and subsequent decrease of the polarization for positive and negative pulse trains, which results from the continuous switching of polarization using pulse width near the characteristics time. The exponential coefficients used to describe the potentiation/depression curves are 1.2/1.8, using equations described elsewhere.[74] In Fig. 3(f), the increase and further decrease ΔP is shown using pre- and post-voltage synaptic like pulses (inset) of 750 ns full width at half maximum (FWHM) and different delay time (Δt) between them. Shorter pulses are shown in supplementary material S15. Large positive (negative) modulation of ΔP for negative (positive) Δt is observed. The shape of the curves is not symmetric, and they are shifted along ΔP due to the presence of imprint as already discussed. The exponential fits[74] for positive and negative Δt are 800 and 400 ns. The exploratory characterization shown in Fig. 3(e) and 3(f) demonstrates the potentiality of the system to show synaptic like behavior, but in a time scale much shorter than that usually measured in polycrystalline doped-HfO_2 films.[14,46,74] The integration of the material in tunnel junctions[14] or transistor or Schottky junctions[46] would allow the fast modulation of conductance mimicking brain behavior at a fast speed.

CONCLUSIONS

In conclusion, the characterization of the switching dynamics in single orthorhombic phase films has allowed us to identify Kolmogorov–Avrami–Ishibashi-like domain switching growth even using low voltage pulses. However, slow τ_0 indicates that ferroelectric switching is somehow intertwined to ionic motion processes. These results contribute to the fundamental understanding of the switching dynamics in ferroelectric hafnium oxide and are relevant for applications. In contrast, we have observed that in films with the presence of parasitic monoclinic phase or in fatigued films, defects and non-ferroelectric phases help to shorten τ_0. Therefore, even limited by the used experimental setup, ferroelectric switching as fast as 50 ns is observed. Fast switching is only observed when the final polarization state is aligned with the imprint field. In the latter case, ionic motion is unlikely to dominate in the switching dynamics due to its fast response, although its local presence at interfaces cannot be disregarded. Potentiation/depression and STDP preliminary data allow us to demonstrate the potential interest in ferroelectric HfO_2 for fast neuromorphic memory applications.

EXPERIMENTAL METHODS

X-ray diffraction characterization has been performed by means of 2θ-χ maps (2θ from 20° to 50°, χ from around −20° to +20°) collected with a Bruker D8-Advance diffractometer using a 2D detector.

Ferroelectric and switching spectroscopy characterization was performed using a TFAnalyser2000 platform (Aixacct Gmbh), grounding the LSMO bottom electrode and biasing one of the top Pt electrodes. Ferroelectric loops were collected using the PUND technique,[53] using triangular pulses at 10 kHz and delay time between pulses of 1 s. Displayed PUND loops are obtained after subtraction of the current measured during the U(D) pulse to the P(N) one. STDP measurements were done applying pre- and post-synaptic pulses of opposite sign to the top Pt electrode after its sum.

SUPPLEMENTARY MATERIAL

See the supplementary material for additional electrical characterization, description of methods, and data analysis.

ACKNOWLEDGMENTS

Financial support from the Spanish Ministry of Science and Innovation (MCIN/AEI/ 10.13039/501100011033), through the Severo Ochoa FUNFUTURE (CEX2019-000917-S), PID2020-112548RB-I00 and PID2019-107727RB-I00 projects, and from CSIC

© Author(s) 2022

through the i-LINK (Grant No. LINKA20338) program is acknowledged. This project was supported by a 2020 Leonardo Grant for Researchers and Cultural Creators, BBVA Foundation. I.F. acknowledges Ramón y Cajal, Contract No. RYC-2017-22531. T.S. was financially supported by the China Scholarship Council (CSC, Grant Nos. 201807000104). T.S. work has been done as a part of his Ph.D. program in Materials Science at Universitat Autònoma de Barcelona.

AUTHOR DECLARATIONS

Conflict of Interest

The authors declare no conflict of interest.

DATA AVAILABILITY

The data that support the findings of this study are available from the corresponding author upon reasonable request.

REFERENCES

[1] T. Böscke *et al.*, Appl. Phys. Lett. **99**, 102903 (2011).
[2] T. Mikolajick *et al.*, MRS Bull. **43**, 340 (2018).
[3] M. H. Park *et al.*, MRS Bull. **46**, 1071 (2021).
[4] T. Schenk *et al.*, Rep. Prog. Phys. **83**, 086501 (2020).
[5] H. Mulaosmanovic *et al.*, Nat. Electron. **3**, 391 (2020).
[6] S. J. Kim *et al.*, Appl. Phys. Lett. **112**, 172902 (2018).
[7] S. Migita *et al.*, Jpn. J. Appl. Phys. **57**, 04FB01 (2018).
[8] J. Lyu *et al.*, ACS Appl. Electron. Mater. **1**, 220 (2019).
[9] M. H. Park *et al.*, Appl. Phys. Lett. **107**, 192907 (2015).
[10] A. Chernikova *et al.*, Microelectron. Eng. **147**, 15 (2015).
[11] M. Hyuk Park *et al.*, Appl. Phys. Lett. **102**, 242905 (2013).
[12] S. S. Cheema *et al.*, Nature **580**, 478 (2020).
[13] M. C. Sulzbach *et al.*, Adv. Funct. Mater. **30**, 2002638 (2020).
[14] B. Max *et al.*, ACS Appl. Electron. Mater. **2**, 4023 (2020).
[15] U. Schroeder *et al.*, *Ferroelectricity in Doped Hafnium Oxide: Materials, Properties and Devices* (Woodhead Publishing, 2019).
[16] T. Mikolajick *et al.*, J. Appl. Phys. **129**, 100901 (2021).
[17] D. H. Lee *et al.*, Appl. Phys. Rev. **8**, 021312 (2021).
[18] H. Mulaosmanovic *et al.*, ACS Appl. Mater. Interfaces **9**, 3792 (2017).
[19] S. D. Hyun *et al.*, ACS Appl. Mater. Interfaces **10**, 35374 (2018).
[20] P. Buragohain *et al.*, Appl. Phys. Lett. **112**, 222901 (2018).
[21] N. Gong *et al.*, Appl. Phys. Lett. **112**, 262903 (2018).
[22] T. Y. Lee *et al.*, ACS Appl. Mater. Interfaces **11**, 3142 (2019).
[23] Y. Li *et al.*, Appl. Phys. Lett. **114**, 142902 (2019).
[24] S.-N. Choi *et al.*, Ceram. Int. **45**, 22642 (2019).
[25] H. Liu *et al.*, Adv. Sci. **7**, 2001266 (2020).
[26] K. Lee *et al.*, Sci. Rep. **11**, 6290 (2021).
[27] U. Schroeder *et al.*, ECS J. Solid State Sci. Technol. **2**, N69 (2013).
[28] M. Si *et al.*, Appl. Phys. Lett. **115**, 072107 (2019).
[29] X. Lyu *et al.*, presented at the 2019 IEEE Int. Electron Devices Meeting (IEDM), 2019.
[30] C. Alessandri *et al.*, IEEE Electron Device Lett. **39**, 1780 (2018).
[31] J. P. B. Silva *et al.*, ACS Appl. Mater. Interfaces **13**, 51383 (2021).
[32] J. P. B. Silva *et al.*, Ceram. Int. **48**, 6161 (2021).
[33] A. K. Tagantsev *et al.*, Phys. Rev. B **66**, 214109 (2002).
[34] M. Avrami, J. Chem. Phys. **9**, 177 (1941).
[35] Y. Ishibashi *et al.*, J. Phys. Soc. Jpn. **31**, 506 (1971).
[36] W. Li *et al.*, Appl. Phys. Lett. **91**, 262903 (2007).
[37] B. Buyantogtokh *et al.*, J. Appl. Phys. **129**, 244106 (2021).
[38] I. Stolichnov *et al.*, Appl. Phys. Lett. **117**, 172902 (2020).
[39] C. Gastaldi *et al.*, Appl. Phys. Lett. **118**, 192904 (2021).
[40] I. Stolichnov *et al.*, ACS Appl. Mater. Interfaces **10**, 30514 (2018).
[41] X. Xu *et al.*, Nat. Mater. **20**, 826 (2021).
[42] I. Fina *et al.*, ACS Appl. Electron. Mater. **3**, 1530 (2021).
[43] P. Buragohain *et al.*, Adv. Funct. Mater. **4**, 2108876 (2021).
[44] Y. Wei *et al.*, Nat. Mater. **17**, 1095 (2018).
[45] J. Lyu *et al.*, Appl. Phys. Lett. **113**, 082902 (2018).
[46] H. Y. Yoong *et al.*, Adv. Funct. Mater. **28**, 1806037 (2018).
[47] T. Li *et al.*, ACS Appl. Mater. Interfaces **11**, 4139 (2019).
[48] B. Prasad *et al.*, Adv. Electron. Mater. **7**, 2001074 (2021).
[49] S. Estandía *et al.*, J. Mater. Chem. C **9**, 3486 (2021).
[50] S. Estandía *et al.*, ACS Appl. Electron. Mater. **1**, 1449 (2019).
[51] T. Song *et al.*, ACS Appl. Electron. Mater. **2**, 3221 (2020).
[52] M. C. Sulzbach *et al.*, Adv. Electron. Mater. **6**, 1900852 (2019).
[53] I. Fina *et al.*, J. Appl. Phys. **109**, 074105 (2011).
[54] G. Bersuker *et al.*, J. Appl. Phys. **110**, 124518 (2011).
[55] M. Lanza *et al.*, Appl. Phys. Lett. **101**, 193502 (2012).
[56] S. Duenas *et al.*, Microelectron. Eng. **216**, 111032 (2019).
[57] Y. W. So *et al.*, Appl. Phys. Lett. **86**, 092905 (2005).
[58] T. H. Kim *et al.*, Appl. Phys. Lett. **99**, 012905 (2011).
[59] M. Pešić *et al.*, Adv. Funct. Mater. **26**, 4601 (2016).
[60] E. D. Grimley *et al.*, Adv. Electron. Mater. **2**, 1600173 (2016).
[61] J. Jo *et al.*, Phys. Rev. Lett. **99**, 267602 (2007).
[62] D. Pantel *et al.*, J. Appl. Phys. **107**, 084111 (2010).
[63] M. D. Glinchuk *et al.*, J. Alloys Compd. **830**, 153628 (2020).
[64] P. Nukala *et al.*, Science **372**, 630 (2021).
[65] S. Santucci *et al.*, J. Mater. Chem. A **8**, 14023 (2020).
[66] S. Zafar *et al.*, Appl. Phys. Lett. **98**, 152903 (2011).
[67] K. Park *et al.*, J. Electrochem. Soc. **138**, 1154 (1991).
[68] M. P. Mueller *et al.*, J. Appl. Phys. **129**, 025104 (2021).
[69] Y. Wei *et al.*, npj Quantum Mater. **4**, 62 (2019).
[70] Y. Goh *et al.*, Appl. Phys. Lett. **117**, 242901 (2020).
[71] Y. Goh *et al.*, ACS Appl. Mater. Interfaces **12**, 57539 (2020).
[72] Y. Goh *et al.*, Nanotechnology **29**, 335201 (2018).
[73] H. Ryu *et al.*, Sci. Rep. **9**, 20383 (2019).
[74] S. Saïghi *et al.*, Front. Neurosci. **9**, 51 (2015).

© Author(s) 2022